Texture formation in sputter-deposited $(Nb_{0.7},Ti_{0.3})N$ thin films

N. N. Iosad[a)]
Department of Applied Physics (DIMES), Delft University of Technology, Lorentzweg 1, 2628 CJ Delft, The Netherlands

N. M. van der Pers
Laboratory for Materials Science, Delft University of Technology, Rotterdamseweg 137, 2628 AL Delft, The Netherlands

S. Grachev
Nuclear Solid State Physics, University of Groningen, Nijenborgh 4.13, 9747 AG Groningen, The Netherlands

V. V. Roddatis[*]
Department of Inorganic Chemistry, Fritz Haber Institute of the Max Planck Society, Faradayweg 4-6, D-14195, Berlin, Germany

B. D. Jackson
SRON, National Institute for Space Research, P.O. Box 800, 9700 AV Groningen, The Netherlands

S. N. Polyakov
Institute of Nuclear Physics, Moscow State University, 119899, GSP, Moscow, Russia

P. N. Dmitriev
Institute of Radioelectronics Russian Academy of Sciences, Mokhovaya 11, 103907, GSP-3, Moscow, Russia

T. M. Klapwijk
Department of Applied Physics (DIMES), Delft University of Technology, Lorentzweg 1, 2628 CJ Delft, The Netherlands

(Received 12 December 2001; accepted 9 August 2002)

We studied the properties of $(Nb_{0.7},Ti_{0.3})N$ films deposited by reactive magnetron sputtering in an atmosphere of argon and nitrogen at ambient substrate temperature, with a particular focus on the technological factors that determine film texture. The texture in the nitrides of transition metals determines many processes, including the wear resistance of tool coatings, diffusion in microelectronic devices, and the rate of chemical etching. Thus, since our goal is to use $(Nb_{0.7},Ti_{0.3})N$ films in superconducting microelectronic devices, texture control is an essential element of our technology. We find that increasing the total gas pressure, while keeping the film chemical composition constant, results in a decrease in the ratio of the [200] and [111] x-ray diffraction (XRD) line intensities on Θ–2Θ Bragg–Brentano scans. Similar changes in XRD patterns are observed as the nitrogen injection increases for a constant sputtering pressure. In addition, XRD examination shows that some samples have in-plane texture developed due to self-shadowing during growth. Transmission electron microscopy reveals that all of the films consist of textured, elongated grains. Analyzing the experimental data, it is concluded that the thermalization of the sputtering yield determines the process of texture formation in the experiment with pressure variation, with an increase in adatom energy resulting in a change in texture from [111] to [100]. However, adatom energy is not the only determining factor—the nitrogen concentration in the sputtering gas also has a strong impact on the film texture. In particular, despite the fact that an increase in nitrogen injection results in an increase in adatom energy, the film texture is driven toward [111]. © *2002 American Institute of Physics.* [DOI: 10.1063/1.1510589]

I. INTRODUCTION

Interest in the analysis of texture formation in $(Nb_{0.7},Ti_{0.3})N$ films is motivated by a need to develop a reliable production line for THz superconducting–insulator–superconducting mixers.[1–8] Because reactive ion-etching rates depend strongly upon the crystallographic plane exposed to the plasma, this article focuses on determining the technological factors that control texture formation. The material of interest has a B1 rock-salt cubic crystal structure, a class of material for which many researchers have observed similar dependences of texture on growth conditions in the past.[1–15] However, only a few manuscripts are dedicated to a detailed texture characterization and an analysis of the technological factors determining the texture. In this article, we present a characterization of various factors contributing to texture formation in our films, and relate the results to existing models.

[a)]Electronic mail: iosad@tnw.tudelft.nl
*On leave from Institute of Crystallography Russian Academy of Sciences, Leninsky pr. 59, 117333 Moscow, Russia.

The question of whether a process reaches equilibrium or is instead limited by kinetics often arises in thin-film growth.[10] In general, there are two contradicting concepts, based on either a thermodynamic or a kinetic approach, which try to explain the formation of texture in the B1-type nitrides of transition metals.[11]

Pelleg *et al.*[12] propose a thermodynamic approach. They state that the degree of surface energy (S_{hkl}) is $S_{100}<S_{110}<S_{111}$, while the degree of strain energy per unit volume, (u_{hkl}), is $u_{111}<u_{110}<u_{100}$. Thus, if one assumes that the surface energy does not depend on film thickness and that the strain energy increases with it, one can then determine the total of the surface energy and strain energy for a given plane (*hkl*). Due to the driving force to minimize the total energy of the system, it would then be expected that [100] texture is preferred for relatively thin films, when the strain energy is less than the surface energy, with a change in texture with increasing film thickness to [110] and ultimately to [111] as the strain energy starts to play a more dominant role in the determination of the total energy. This theoretical prediction of the formation of strain-minimizing textures during film thickening is supported by the recent experimental observations of Oh and Je[13] for 1.5 μm thick TiN films deposited by reactive rf-magnetron sputtering in a pure nitrogen atmosphere.

In contrast, Greene *et al.*[14] state that texture can be determined by kinetic effects such as incident particle distributions, nitrogen overpressure, orientation-dependent surface adatom mobility, etc.[14] In particular, they have shown that the presence of strain and/or changes in the state of strain throughout the film thickness are not requirements for obtaining changes in preferred orientation. We have proposed in previous work, that adatom energy may be a key parameter of film growth in the case of magnetron sputtering at ambient substrate temperature.[8] Petrov *et al.*[15] associate changes in the texture of rf-bias-sputtered TiN films with ion channeling. In this case, they explain a change from [111] to [100] texture with an increase in ion assistance by the fact that the planes corresponding to easy ion channeling and lower sputtering yields have the highest probability to survive. Many researchers use an approach based on the ratio of the growth rates of different facets.[16–19] For example, for a cubic lattice, an increase in the ratio of the {100} and {111} facet growth rates results in a transition of texture from [100] to [110], and finally to [111]. (It is interesting to note that the texture evolution in this case is the same as in the thermodynamic model.) Thus, a transition from [111] to [110] texture occurs via an abundance of [11γ] textures, while the transition from [110] to [100] texture occurs via an abundance of [1γ0] textures, where $0\leqslant\gamma\leqslant1$. Despite the apparent simplicity of this approach, factors like crystallographic defects, a lack of surface diffusion, or an instrumental function of the growth apparatus, etc., may hamper the growth of particular facets and cause the crystal habit and film texture to differ from the one expected from the ratio of the {111} and {100} facet growth rates.[20] For example, a number of experimental reports are dedicated to specific in-plane orientations that are favored during thickening.[21–24] This phenomenon may take place in magnetron deposition if the product of the sputtering pressure and substrate–target distance is small. In this case, the trajectories of sputtered particles are almost ballistic, and the crystal facets facing the flux of the particles grow faster.[11] Finally, one of the most detailed studies of film texture and its correlation with the intensity and angle of incidence of the ion-beam bombarding the surface of the growing film was performed by Alberts *et al.*[25] Their study of biaxially textured films shows that none of the aforementioned models can satisfactorily explain their experimental data.

II. EXPERIMENT

Films of $(Nb_{0.7},Ti_{0.3})N$ are deposited by reactive magnetron sputtering in a Nordiko-2000 sputtering system with a base pressure of 4×10^{-5} Pa. This sputtering machine is equipped with a cryopump and a throttling valve, which together determine the process pressure, while the injection of Ar and N_2 gases is controlled by flow meters. In order to avoid the hysteretic sputtering regime, the pumping rate is fixed at a high value of 750 l/s for all experiments.[26] Because the nitrogen injection is more than ten times lower than the argon injection in all experiments, the target material is primarily sputtered by argon atoms. A 99.8% pure alloy target with 30 at. % Ti and 70 at. % Nb is used. All films are sputtered by 300 W dc power and have a thickness of 480 $\pm$20 nm. Wafers are fixed to the copper chuck (maintained at 20 °C) with diffusion pump oil to stabilize the substrate temperature. A detailed description of the home-made 3 in. circular sputtering source used for film deposition is published in Ref. 8. Ion assistance produced by this sputtering source has only a moderate influence on the film properties when compared with the changes caused by variations in sputtering pressure.[8] Gas densities are measured by inserting a small sampling pipe (attached to an external pressure gauge) between the sputtering source and the substrate. The details of this technique are discussed in the work of Rossnagel.[27]

Films are deposited on 2 in. oxidized Si wafers. The center of the substrate chuck is located exactly below the center of the sputtering source and both the position of the substrate on the chuck and the area of the substrate where measurements are made are carefully monitored to reveal the influence of technological factors that are responsible for in-plane texture formation. In all of the experiments described here, the center of the wafer is located 0.5 in. from the chuck center, unless specifically mentioned in the text. The central part of the wafer (approximately 1 in. in diameter) is used for all measurements. Note that this method of substrate loading allows us to determine the contribution of self-shadowing effects to texture formation, as it is quite clear that self-shadowing effects will increase with increasing offset of the substrate from the center of the chuck, and will have azimuthal symmetry with respect to the center of the substrate chuck.

The stress in the films is evaluated by measuring the deflection of the wafer before and after film deposition with a profilometer. Assuming that the film thickness is much less than the substrate thickness, the film stress is then calculated

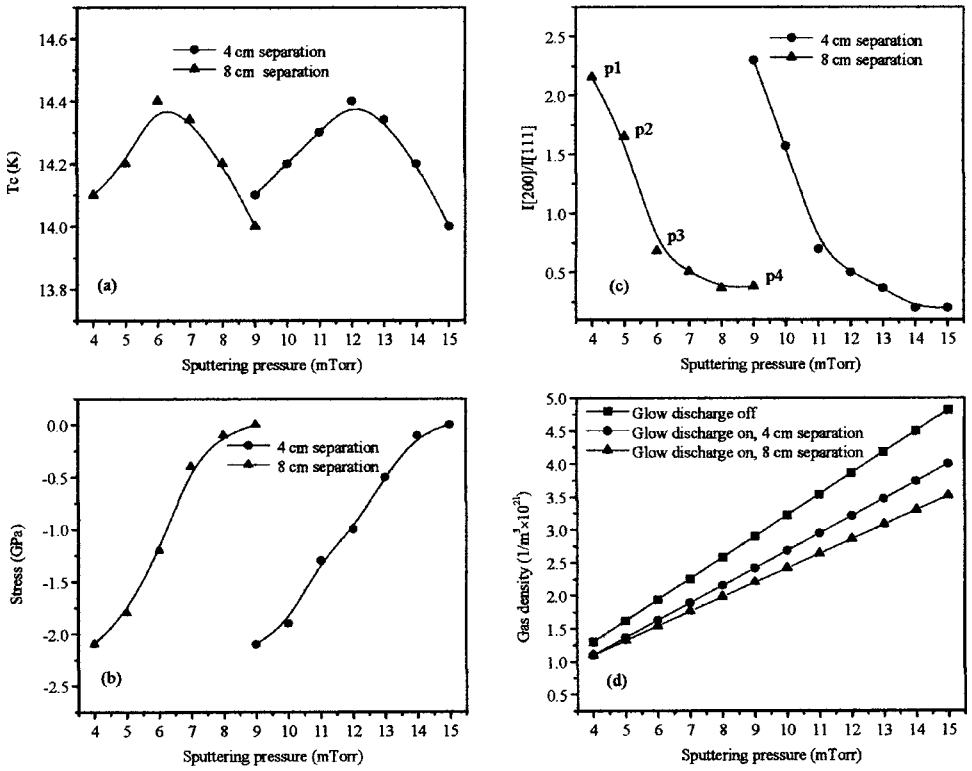

FIG. 1. T_c, intrinsic stress, ratio of [200] and [111] XRD peaks, and gas density between the sputtering source and substrate, for films sputtered at different pressures and maximum (8 cm) and minimum (4 cm) substrate–target separation [(a)–(d), respectively]. Texture examination is carried out for the samples marked p1–p4 on the top right-hand side plot.

using Stoney's equation,[28] with Young's modulus and Poisson's ratio taken from Ref. 29. The transition temperature (T_c) is evaluated from the dependence of film resistivity on temperature. Film chemical composition is measured by Rutherford backscattering spectroscopy (RBS) using a 1 MeV He^+ beam for sample irradiation, while phase identification is based on x-ray diffraction (XRD) scans using a Rigaku D/max-Rc diffractometer. Texture measurements are performed with a Bruker-AXS D5005 diffractometer. Since most of our samples have a rotational symmetry of texture, a simple Ψ-scan procedure (a radial cross section of the pole figure space) is also used for texture characterization. Cross-sectional transmission electron microscopy (TEM) samples are prepared by a standard technique—mechanical thinning down to 30 μm, followed by ion milling using a Gatan Precision Ion Polishing System. The specimens are examined with a Philips CM200ST transmission electron microscope operated at 200 kV. Further details of the RBS, XRD, and TEM analysis methods are published elsewhere.[6]

A. Film properties versus sputtering pressure

We have optimized the nitrogen injection for a wide range of total sputtering pressures in order to maximize the T_c of the $(Nb_{0.7},Ti_{0.3})N$ films. The limits of the pressure range used are determined by film degradation caused by destructive bombardment of the growing film by fast neutrals at low pressures, and high thermalization conditions at high pressures.[6] Figure 1 contains two sets of data for films deposited at the minimum substrate–target distance (4 cm) and the maximum substrate–target distance (8 cm). The deposition rates are 180 ± 10 nm/min and 80 ± 5 nm/min, respectively. XRD analysis shows that all of the films have a B1 crystal structure and both sets of data show similar behavior versus sputtering pressure. In general, the T_c of the films is seen to have only a moderate dependence on the sputtering conditions, illustrating the well-known insensitivity of this value to structural defects in the B1 superconductors [Fig. 1(a)]. Compressive stress also shows a typical behavior versus sputtering pressure for magnetron sputtering systems: It decreases significantly with increasing sputtering pressure [Fig. 1(b)]. The variation in the intensity ratio of the [200] and [111] XRD lines indicates a substantial changes in the film structure [Fig. 1(c)]. Finally, gas rarefaction becomes less pronounced at low pressures, since the hot particles of the sputtering yield have fewer collisions with the cold gas particles than at high pressures [Fig. 1(d)]. Furthermore, because gas cooling during sputtering is more effective at the minimum substrate–target distance (due to an instrumental function of the sputtering system), gas rarefaction is weaker in this case. Note that RBS indicates that all films have almost stoichiometric composition, with a metal–nonmetal concentration ratio of 1 ± 0.03, and a ratio of Nb and Ti in the deposited films that is the same as in the target.

B. Film properties versus nitrogen injection

In this second experiment, the nitrogen injection is varied, while keeping the total sputtering pressure fixed at 6 mTorr. The substrate–target distance is set to the maximum distance (8 cm), and the limits of nitrogen injection are determined by a requirement that a B1-type crystal structure is produced. The resulting deposition conditions and film properties are illustrated in Fig. 2. As in the first experiment, T_c is seen to have a moderate dependence on nitrogen injection [Fig. 2(a)]. Compressive stress has only a moderate increase with nitrogen injection [Fig. 2(b)]. This is presumably due to

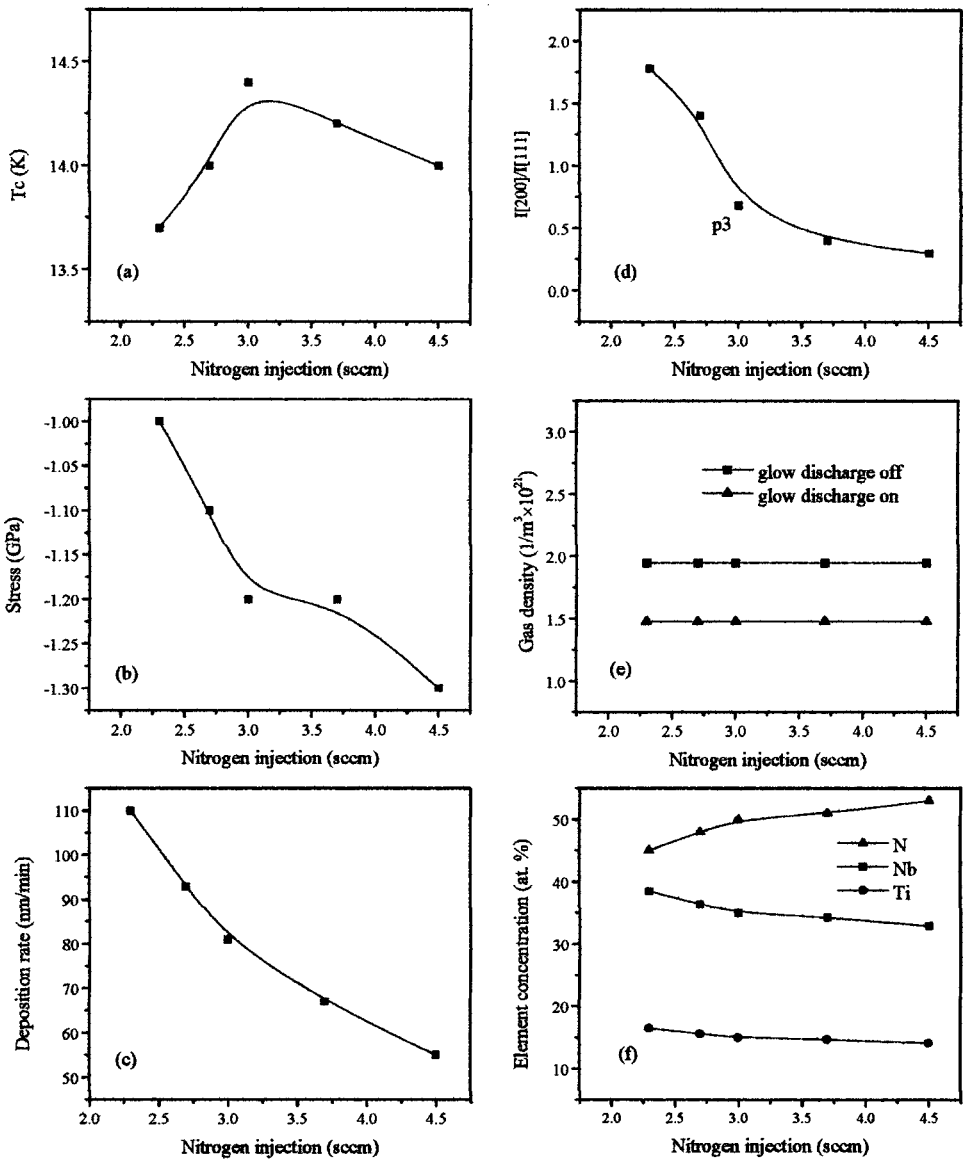

FIG. 2. T_c, intrinsic stress, deposition rate, ratio of [200] and [111] XRD peaks, gas density between the sputtering source and substrate, and chemical composition of the films sputtered at 6 mTorr sputtering pressure for various values of nitrogen injection [(a)–(f), respectively]. The substrate–target distance is set to the maximum (8 cm). The data point marked as p3 on the top right-hand side plot corresponds to a film sputtered under 6 mTorr sputtering pressure and maximum separation in the experiment with pressure variation (Fig. 1).

the fact that the fluxes of ions and fast neutrals bombarding the substrate surface are nearly independent of nitrogen injection, so that a reduction in deposition rate results in an increase in the effective intensity of the fluxes responsible for Ar peening. [Note that Fig. 2(c) shows that the deposition rate decreases with an increase in nitrogen injection, as is expected in reactive sputtering.] The most notable feature in these results is that the ratio of the [200] and [111] XRD peak intensities decreases strongly with increasing nitrogen injection [Fig. 2(d)], which is a clear indication that substantial changes in film texture also take place in this experiment. Despite the fact that the deposition rate decreases with an increase in nitrogen injection, gas rarefaction does not change [Fig. 2(e)], which is a clear indication that the particles of the sputtering yield become more energetic with an increase in nitrogen injection, causing the same gas rarefaction despite a reduction in numbers.[30] (Note that Rossnagel reports similar results[27]—he shows that the degree of gas rarefaction caused by the flux of hot sputtered particles depends mainly on the applied power, and that the target material has almost no influence on this phenomenon.) Finally, it is found that increasing the nitrogen injection by a factor of 2 results in only a moderate increase in the nitrogen concentration in the films [Fig. 2(f)], indicating that we are operating in the sputtering regime in which the target surface is coated with nitride, and changes in nitrogen injection result primarily in a different depth of target nitridation.[31,32]

C. Film texture determination and analysis

Four samples, marked as p1–p4 in Fig. 1(c), are selected for texture examination in the experiment with sputtering pressure variation and maximum substrate–target separation. Because samples p1, p2, and p4 have a rotational symmetry of their texture, an illustration of only one Ψ-scan is sufficient, and they will be discussed first. Sample p1 has a well-pronounced [100] texture [Fig. 3(a)]. [The peak in the 111 intensity curve at $\sim 50°$ corresponds with the angle between the {111} and {100} planes in the face-centered-cubic (fcc) lattice.] In contrast, sample p4 has a distinct [111] texture [Fig. 3(d)]. (The peak in the 200 intensity curve at $\Psi = 50°$ is due to the same reason. Likewise, the peak in the 111 inten-

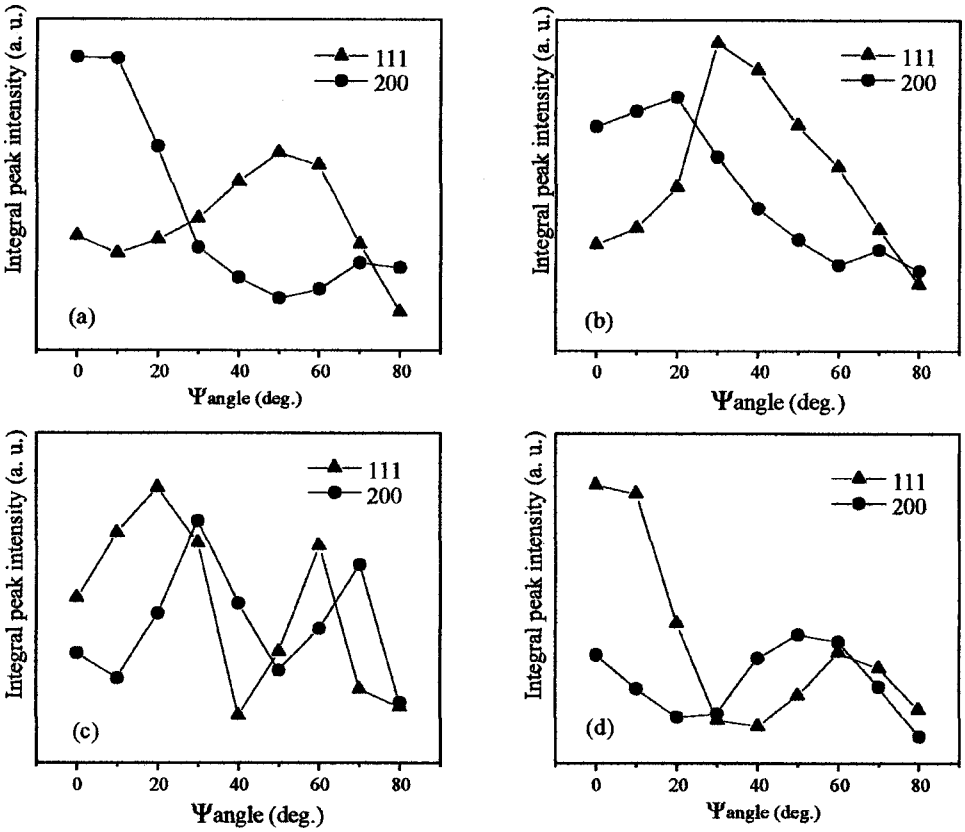

FIG. 3. Ψ-scans of samples p1–p4 [(a)–(d), respectively]. $\Psi=0$ corresponds to the direction perpendicular to the substrate surface.

sity curve at ~70° is due to the fact that the angle between {111} equivalent planes is 70.4°.) Sample p2 consists of a mixture of [100] and [311] textured grains [Fig. 3(b)]. (The intense peak at $\Psi=30°$, with a stretched shoulder toward $\Psi=80°$ on the 111 intensity curve is due to the merging of peaks of [311] textured grains at $\Psi=29.5°$ and 58.5°, plus a peak of [100] textured grains at $\Psi=54.7°$. Similar reasons cause peaks on the 200 intensity curve at $\Psi=20°$ and 70°.)

Sample p3 does not have a rotational symmetry of texture. For this reason, a pole figure of the [111] reflection of sample p3 and its location on the substrate chuck are illustrated in Figs. 4(a) and 4(c), respectively. It is seen that sample p3 has an in-plane texture that is oriented in the direction of vector **R**, which starts in the center of the chuck and goes through the center of the measurement zones. In order to verify the hypothesis that self-shadowing is the cause of this in-plane texturing, we have deposited sample p3a under the same conditions as sample p3, but with a larger off-center loading position [see Fig. 4(c)]. This sample is found to show a more pronounced in-plane texture, because the sputtering yield flux is more oblique [Fig. 4(b)]. Samples p3 and p3a have $[211](\bar{1}11)$ texture, since they have maximum intensities at $\Psi\approx20°$ and $\varphi\approx0°$, $\Psi\approx60°$ and $\varphi\approx110°$, and $\Psi\approx60°$ and $\varphi\approx250°$. Finally, in order to illustrate the dependence of texture evolution on sputtering pressure, Fig. 3(c) shows a Ψ-scan of sample p3. This Ψ-scan is made in the direction perpendicular to the radius vector **R**, in order to minimize the contribution of the self-shadowing effect. The peaks at $\Psi=30°$ and 60° on the 200 intensity curve correspond with the angles between the {100} and {211} planes. Reflections of [211] textured grains also cause peaks on the {111} intensity curve at $\Psi=20°$ and 60°.

The fact that we observe in-plane texture for sample p3 only in the experiment with pressure variation and a maximum substrate–target distance is attributed to a balance between two factors in this case. On one hand, the film roughness decreases with decreasing sputtering pressure, suppressing self-shadowing. This reduction in surface roughness can be observed by the naked eye: the film color changes from dark to light yellow as the sputtering pressure decreases, due to a different crystal habit of [111] and [100] textured grains. Similar results are observed in computer simulations and experimental investigations.[17,33] (Note that the [100] textured grains have an almost flat surface in comparison with the [111] textured grains.) On the other hand, reducing the sputtering pressure makes the flux of the sputtered particles less diffuse, which facilitates self-shadowing. As a result of the balance between these two factors, the in-plane texture is only observed for the sample p3.

Although not shown here, a similar texture dependence on sputtering pressure is observed at the minimum substrate–target distance. Likewise, examining the film texture versus nitrogen injection shows a similar texture evolution. In particular, a detailed examination of the texture reveals that the film deposited with the lowest nitrogen injection has a texture similar to the texture of sample p2, while the film deposited with the highest nitrogen injection has a texture similar to that of sample p3. In other words, increasing the nitrogen injection affects the film texture in the same way as an increase in sputtering pressure.

A cross-sectional TEM image of the film sputtered under a total pressure of 6 mTorr and 3 sccm nitrogen injection

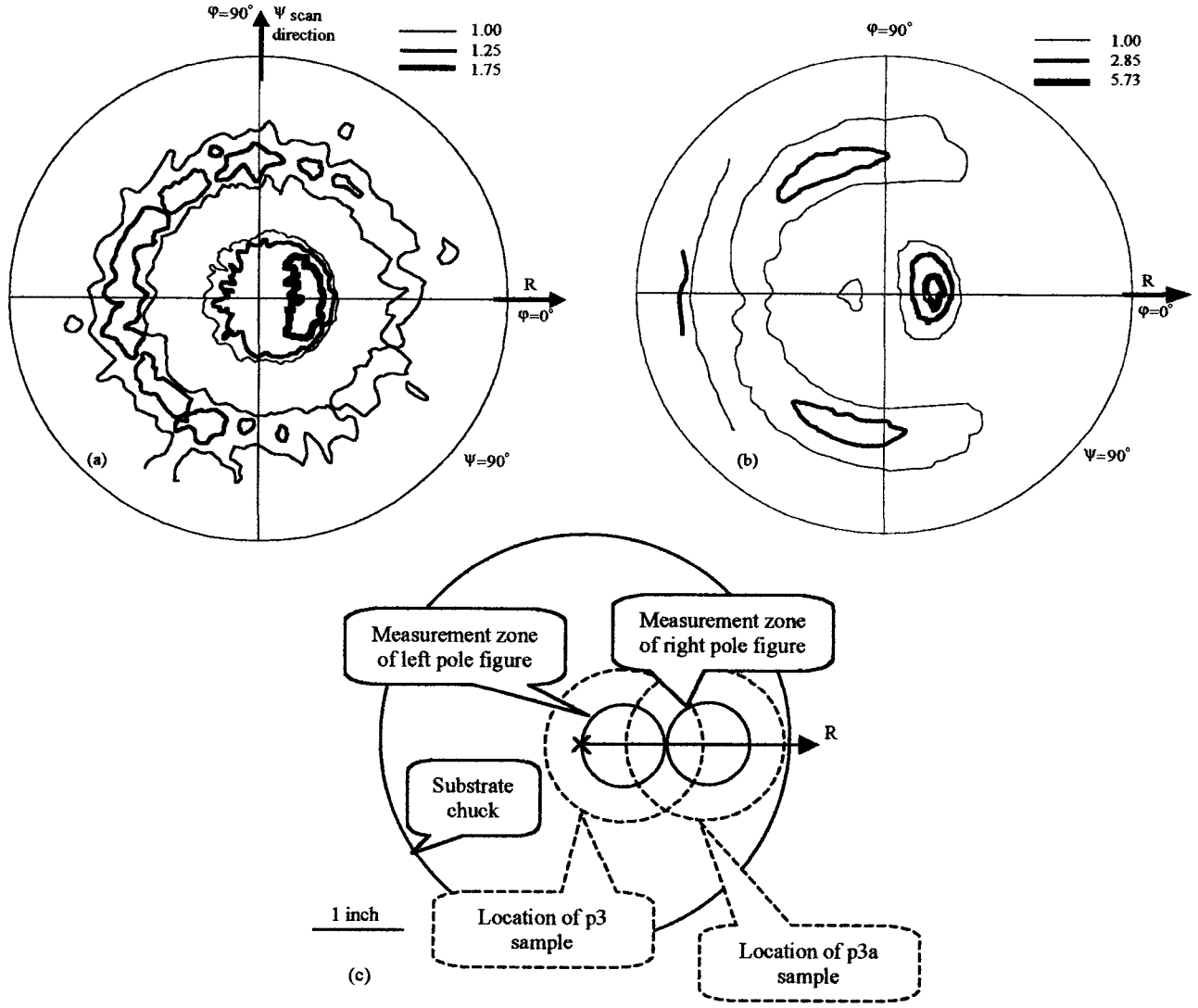

FIG. 4. Pole figures of [111] reflections of samples p3 [(a)] and p3a [(b)], plus a schematic diagram illustrating the locations of the wafers and measurement zones on the substrate chuck [(c)].

(sample p3 in Figs. 1 and 2) is shown in Fig. 5. The cross section is made in the same plane as the Ψ-scan (Fig. 4). A selective area diffraction pattern is also shown in the insert of Fig. 5(a), revealing also the presence of a weak texture indicated by intensity variations in the diffraction rings. The [111] reflection from the grain marked with an arrowhead in Fig. 5(a) is used to make a dark-field image [Fig. 5(b)] to illustrate the morphological texture. From the results in Fig. 5, it is seen that the in-plane grain size increases with film thickness as a result of competitive growth.[9,34] The image illustrated in Fig. 5 is typical for all of the studied films. It is interesting to note that, in contrast with the case of texture determined by competitive growth that is mentioned in the introduction, the change from [111] to [100] texture goes via the abundance of $[1\gamma\gamma]$ textures, where $0 \leqslant \gamma \leqslant 1$. In other words, the system bypasses the [110] texture.

As seen from Figs. 1 and 3, an increase in compressive stress correlates with a change from [111] to [100] texture. Thus, the thermodynamic model does not describe our case, since it predicts the opposite behavior. Furthermore, previous work has shown that ion assistance is quite weak and has a very moderate impact on the properties of these films,[8] allowing us to exclude the ion-channeling approach as well. However, as seen in Fig. 1, the properties of films sputtered at a minimum substrate–target distance are almost equivalent to the properties of films sputtered at maximum substrate–target distance and twice lower gas concentration. This is a clear indication that the thermalization of the sputtering yield is one of the determining factors in the process of texture formation (i.e., the energy of the adatom is a critical factor in this process).[35] Increasing the adatom energy causes a change in texture from [111] to [100] in the experiment with pressure variation. This experiment also indicates that there is no dependence of film properties on deposition rate, in contrast with results reported by Deen.[36] This means that surface diffusion is not suppressed by increasing the adatom arrival rate.[37] Finally, the fact that the system is driven toward [111] texture with increasing nitrogen injection, despite an increase in adatom energy, shows that the chemical composition of the film also plays a very strong role in texture formation in these films.

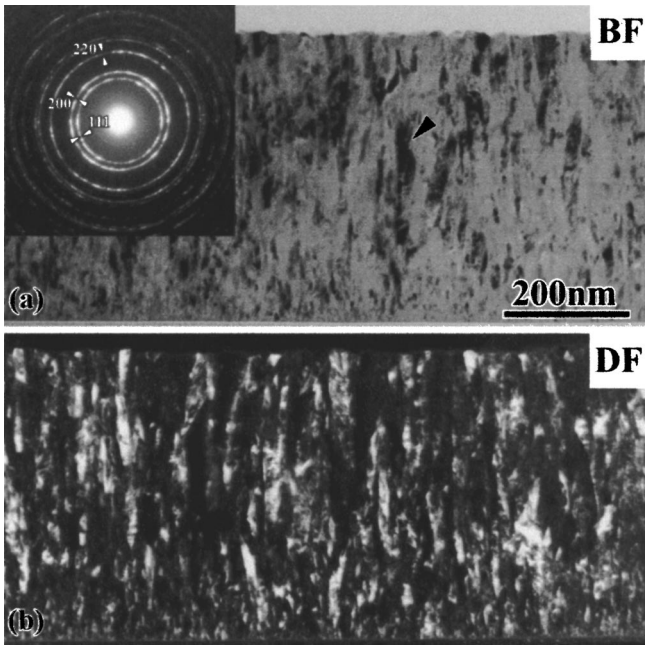

FIG. 5. Cross-sectional TEM images in the bright [(a)] and dark [(c)]. fields of sample p3. A selected area diffraction image is shown in the inset of (a).

III. CONCLUSIONS

The texture of $(Nb_{0.7},Ti_{0.3})N$ films is examined over a wide range of technological parameters. Film chemical composition, adatom energy, and crystal habit are identified as determining factors for texture formation and the contribution of in-plane texturing due to self-shadowing is identified by off-center substrate loading. Varying the sputtering pressure for different substrate–target distances reveals that increasing the adatom energy results in a change of texture from [111] to [100] for a constant chemical composition. The thermodynamic model, based on a balance of stress energy and surface energy, is not applicable in this case, since minimizing the overall energy predicts a transition from [100] texture to [111] texture as compressive stress increases, while our films show the opposite behavior. In addition, this experiment indicates that deposition rate does not affect the film growth. However the process of texture formation is not exclusively kinetically limited—despite the fact that an increase in nitrogen injection results in an increase in the adatom energy, the system is driven towards [111] texturing. TEM analysis shows that film texture is formed through a process of competitive growth. Furthermore, despite the fact that adatom energy and film chemical composition are factors with different origins, their impacts on film texture evolution are the same. Finally, the transition from [111] to [100] texture occurs via an abundance of $[1\gamma\gamma]$ textures, where $0 \leqslant \gamma \leqslant 1$, while the classical model, based on competitive growth of {111} and {100} facets, predicts a transition from [111] to [110] texture via an abundance of $[11\gamma]$ textures and a transition from [110] to [100] via an abundance of $[1\gamma 0]$ textures. The origin of this difference is yet to be determined.

ACKNOWLEDGMENTS

The authors thank R. Delhez, A. J. Dammers, P. Bronsveld, V. P. Koshelets, E. K. Kov'ev, V. Morozov, and A. H. Verbruggen for helpful discussions. The work was supported in part by ESA Contract No. 11653/95, INTAS Project No. 01-0367, and the RFBR Project No. 00-02-16270. One of the authors (V. V. R.) is indebted to the Max-Planck Society for his fellowship at the Fritz-Haber Institute.

[1] R. Di Leo, A. Nigro, G. Nobile, and R. Vaglio, J. Low Temp. Phys. **78**, 41 (1990).
[2] Y. Uzawa, A. Kawakami, S. Miki, and Z. Wang, IEEE Trans. Appl. Supercond. **11**, 183 (2001).
[3] H. Yamamori and A. Shoji, Supercond. Sci. Technol. **12**, 877 (1999).
[4] J. Kawamura, J. Chen, D. Miller, J. Kooi, J. Zamudzinas, B. Bumble, H. G. LeDuc, and J. A. Stern, Appl. Phys. Lett. **75**, 4013 (1999).
[5] B. D. Jackson, A. M. Baryshev, G. de Lange, J. R. Gao, S. V. Shitov, N. N. Iosad, and T. M. Klapwijk, Appl. Phys. Lett. **79**, 436 (2001).
[6] N. N. Iosad, A. V. Mijiritskii, V. V. Roddatis, N. M. van der Pers, B. D. Jackson, J. R. Gao, S. N. Polyakov, P. N. Dmitriev, and T. M. Klapwijk, J. Appl. Phys. **88**, 5756 (2000).
[7] N. N. Iosad, B. D. Jackson, T. M. Klapwijk, S. N. Polyakov, P. N. Dmitriev, and J. R. Gao, IEEE Trans. Appl. Supercond. **9**, 1716 (1999).
[8] N. N. Iosad, B. D. Jackson, S. N. Polyakov, P. N. Dmitriev, and T. M. Klapwijk, J. Vac. Sci. Technol. A **19**, 1840 (2001).
[9] N. N. Iosad, V. V. Roddatis, S. N. Polyakov, V. V. Varlashkin, B. D. Jackson, P. N. Dmitriev, J. R. Gao, and T. M. Klapwijk, IEEE Trans. Appl. Supercond. **11**, 3832 (2001).
[10] D. L. Smith, *Thin Film Deposition* (McGraw–Hill, New York, 1995), p. 150.
[11] C. V. Thompson, Annu. Rev. Mater. Sci. **30**, 159 (2000).
[12] J. Pelleg, L. Z. Zevin, and S. Lungo, Thin Solid Films **197**, 117 (1991).
[13] U. C. Oh and J. H. Je, J. Mater. Res. **13**, 1225 (1998).
[14] J. E. Greene, J.-E. Sundgren, L. Hultman, I. Petrov, and D. B. Dergstrom, Appl. Phys. Lett. **67**, 2928 (1995).
[15] I. Pertov, L. Hultman, J.-E. Sundgren, and J. E. Greene, J. Vac. Sci. Technol. A **10**, 265 (1992).
[16] J. M. Thijssen, H. J. F. Knops, and A. J. Dammers, Phys. Rev. B **45**, 8650 (1992).
[17] M. Grujicic and S. G. Lai, J. Mater. Sci. **36**, 2937 (2001).
[18] F. Paritosh, D. J. Srolovitz, C. C. Battaile, X. Li, and J. E. Buttler, Acta Mater. **47**, 2269 (1999).
[19] A. J. Dammers and S. Radelaar, Textures Microstruct. **14**, 757 (1991).
[20] Ch. Wild, N. Herres, and P. Koidl, J. Appl. Phys. **68**, 973 (1990).
[21] A. K. Malhotra, S. M. Yalisove, and J. C. Bilello, Thin Solid Films **286**, 196 (1997).
[22] N. Sonnenberg, A. S. Longo, M. J. Cima, B. P. Chang, and K. G. Ressler, J. Appl. Phys. **74**, 1027 (1993).
[23] E. Zoestbergen and J. T. M. De Hosson, Thin Solid Films **371**, 10 (2000).
[24] O. P. Karpenko, J. C. Bilello, and S. M. Yalisove, J. Appl. Phys. **82**, 1397 (1997).
[25] L. Alberts, R. Leutenecker, and G. K. Wolf, Surf. Coat. Technol. **84**, 443 (1996).
[26] K. L. Westra, M. J. Brett, and J. F. Vaneldik, J. Vac. Sci. Technol. A **8**, 1288 (1990).
[27] S. M. Rossnagel, J. Vac. Sci. Technol. A **6**, 19 (1988).
[28] G. C. Stoney, Proc. R. Soc. London, Ser. A **32**, 172 (1909).
[29] W. A. Brantley, J. Appl. Phys. **44**, 534 (1973).
[30] C. Steinbruchel, and D. M. Gruen, J. Vac. Sci. Technol. **18**, 235 (1981).
[31] L. B. Jonsson, T. Nyberg, and S. Berg, J. Vac. Sci. Technol. A **17**, 1827 (1999).
[32] I. Petrov, A. Myers, J. E. Greene, and J. R. Abelson, J. Vac. Sci. Technol. A **12**, 2864 (1994).
[33] L. Hultman, W. D. Munz, J. Musil, S. Kadlec, I. Petrov, and J. E. Greene, J. Vac. Sci. Technol. A **9**, 434 (1991).
[34] L. Hultman, J.-E. Sundgren, J. E. Greene, D. B. Bergstrom, and I. Petrov, J. Appl. Phys. **78**, 5935 (1995).
[35] M. Wittmer, J. Vac. Sci. Technol. A **3**, 1797 (1985).
[36] M. J. Deen, Thin Solid Films **152**, 535 (1987).
[37] D. L. Smith, *Thin Film Deposition* (McGraw–Hill, New York, 1995), p. 135.